

pubs.acs.org/est Article

Microplastics and Nanoplastics Impair the Biophysical Function of Pulmonary Surfactant by Forming Heteroaggregates at the Alveolar—Capillary Interface

Xiaojie Xu, ∇ Ria A. Goros, ∇ Zheng Dong, Xin Meng, Guangle Li, Wei Chen, Sijin Liu, Juan Ma,* and Yi Y. Zuo*



Cite This: Environ. Sci. Technol. 2023, 57, 21050-21060



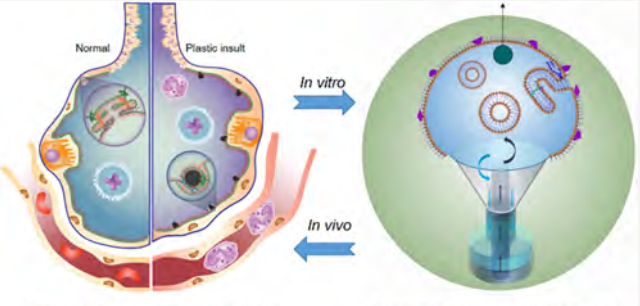
ACCESS I

III Metrics & More

Article Recommendations

Supporting Information

ABSTRACT: Microplastics (MPs) are ubiquitous environmental pollutants produced through the degradation of plastic products. Nanoplastics (NPs), commonly coexisting with MPs in the environment, are submicrometer debris incidentally produced from fragmentation of MPs. We studied the biophysical impacts of MPs/NPs derived from commonly used commercial plastic products on a natural pulmonary surfactant extracted from calf lung lavage. It was found that in comparison to MPs/NPs derived from lunch boxes made of polypropylene or from drinking water bottles made of poly(ethylene terephthalate), the MP/NP derived from foam packaging boxes made of polystyrene showed the highest adverse impact on the biophysical function of the



Micro/nanoplastics-induced lung injury

Constrained drop surfactometry (CDS)

pulmonary surfactant. Accordingly, intranasal exposure of MP/NP derived from the foam boxes also induced the most serious proinflammatory responses and lung injury in mice. Atomic force microscopy revealed that NP particles were adsorbed on the air—water surface and heteroaggregated with the pulmonary surfactant film. These results indicate that although the incidentally formed NPs only make up a small mass fraction, they likely play a predominant role in determining the nano-bio interactions and the lung toxicity of MPs/NPs by forming heteroaggregates at the alveolar—capillary interface. These findings may provide novel insights into understanding the health impact of MPs and NPs on the respiratory system.

KEYWORDS: microplastics, nanoplastics, pulmonary surfactant, constrained drop surfactometry, atomic force microscopy, heteroaggregation

■ INTRODUCTION

Microplastics (MPs), ranging from 1 μ m to 5 mm in size, are predominantly produced through the degradation of plastic products.^{1,2} When exposed to environmental conditions, the structural integrity of plastics is weakened, causing the bulk material to be broken down into smaller pieces.³ This natural weathering process is due to a variety of factors such as UVinduced aging, chemical erosion, and mechanical stress.^{4,5} MPs have been found in all continents, 6,7 worldwide aquatic ecosystems, 8,9 as well as the atmosphere of multiple metropolitan areas. 10,11 Due to the surge in the production of single-use plastics amid the COVID-19 pandemic, escalated concerns are raised for MP accumulation in the environment. 12 Nanoplastics (NPs) are submicron debris incidentally produced from the environmental fragmentation of MPs. 13 Although commonly coexisting with MPs in the environment, due to their small sizes and hence unique colloidal properties, NPs have demonstrated distinct environmental fate and behavior of interaction with biological systems. 14 Nevertheless, like most plastics, MPs and NPs are not biodegradable and,

thus, could take decades or even centuries for complete decomposition. Accordingly, there is an urgent need to understand the environmental, health, and safety (EHS) impacts of MPs/NPs.

Emerging evidence suggested that MPs/NPs can enter the human body through the gastrointestinal portal (via foods, water, and beverages)¹⁵ or the respiratory portal (via aerosols). ^{16,17} Increasing evidence supports that atmospheric fallout is largely responsible for producing airborne MPs. ¹⁸ As a consequence of wind activity, MPs deposited in marine and soil environments can be resuspended into the air, where their small size warrants an extended atmospheric lifetime. ¹⁹ In addition, studies show human activity, wind abrasion, and

Received: August 16, 2023 Revised: November 20, 2023 Accepted: November 21, 2023 Published: December 6, 2023





rainfall increase the amount of airborne MPs detected in indoor and outdoor urban areas. 18,20,21 Once becoming airborne, aerosols in the size range between 0.5 and 5 μm likely bypass mucociliary clearance barriers and penetrate deep into the lung. 22,23 Recent studies have confirmed the presence of MPs in the distal lungs of living humans, in which polyethylene terephthalate and polypropylene were found to be the major active plastic components. 16 MPs were detected in 11 of 13 lung tissue samples from patients undergoing cancer or lung volume reduction surgeries. It was found that the MPs preferentially deposit in the lower lobe of the lung, with an average particle number concentration of 3.12 pieces of MPs per gram of lung tissues. 16 Nevertheless, the actual amount of MPs and NPs in the lung could be even higher since the techniques used in that study can only detect MPs larger than 3 μ m. ¹⁶ In a separate study, it was found that inhalation of MPs originated from tire wear particles may lead to pulmonary fibrosis.2

Once entering the distal lung, the MPs/NPs must first interact with the pulmonary surfactant layer that lines the entire air-water surface of the alveoli as a thin film. The pulmonary surfactant is composed of ~80 wt % phospholipids, 5-10% neutral lipids, and 5-10% proteins. 25 The main biophysical function of the surfactant film is to sustain normal respiration by minimizing the energy required to reinflate the lungs and by reducing surface tension to near-zero values upon expiration.²⁵ The surfactant film also plays an immunological role in host defense against inhaled particles and pathogens at the alveolar–capillary interface. To the best of our knowledge, there are a very limited number of in silico²⁷ and in vitro²⁸ studies that investigated the effect of exposure to MPs/NPs on the biophysical properties of pulmonary surfactants. Using molecular dynamics simulations, Li et al. found that NPs with sizes of 5 and 10 nm could interfere with the biophysical properties of a simulated surfactant film, indicated by disruption of the ultrastructure and fluidity of the surfactant film, and by promotion of film collapse. In an in vitro study, Shi et al. utilized engineered polystyrene microbeads smaller than 1 μ m as model MPs to explore their interactions with a porcine surfactant, employing a Langmuir film model.²⁸ It was found that the engineered polystyrene microbeads altered the phase behavior and surface activity of the surfactant film.²⁸ Although offering some insight into the health impact of MPs/NPs, these studies provided only limited EHS implications because of the use of engineered polymeric spheres/particles as model MPs. It is well known that engineered polymeric micro- or nanoparticles do not represent the heterogeneity of MPs/NPs in composition and morphology.¹⁴ The heterogeneity of MPs in shape and morphology appears to be an important risk factor for their interaction potential with cell membranes²⁹ and their ability to induce cell death.³⁰ Hence, it is still largely unknown how MPs/NPs interact with the surfactant film and how these interactions may adversely affect the respiratory health.

Here, we studied the biophysical impacts of MPs/NPs, derived from commonly used commercial plastic products, on a natural pulmonary surfactant, called Infasurf. Infasurf is a natural surfactant preparation extracted from calf lung lavage.³¹ The composition of bovine surfactant is very similar to that of human surfactant.³² Three representative MP/NP samples produced from commonly used commercial plastic products, broken down, and aged under laboratory conditions were studied.³³ Sources of these MP/NP samples were disposable

lunch boxes made of polypropylene (lunch box-PP), foam packaging boxes made of polystyrene (foam box-PS), and drinking water bottles made of poly(ethylene terephthalate) (water bottle-PET).³³ The biophysical impact of the MPs/NPs on the pulmonary surfactant was evaluated with constrained drop surfactometry (CDS), a novel droplet-based tensiometry technique capable of mimicking the highly dynamic intra-alveolar environment of the lung.³⁴ Proinflammatory responses and lung damage induced by the MPs/NPs were studied by using an intranasal exposure model in mice. To investigate the mechanism of surfactant inhibition and the underlying cause of lung failure, atomic force microscopy (AFM) was employed to directly examine the heteroaggregation of plastic particles with a pulmonary surfactant film.

■ MATERIALS AND METHODS

Pulmonary Surfactant. Infasurf (ONY Biotech, Amherst, NY) is an animal-derived modified natural surfactant. Infasurf was prepared through centrifugation and extraction from the lung lavage of the newborn calves. The extraction process removed the hydrophilic surfactant proteins, SP-A and SP-D, but preserved most hydrophobic components of the bovine surfactant, including the hydrophobic surfactant proteins, SP-B and SP-C.³¹ For storage, Infasurf was deposited into sterilized vials at an initial phospholipid concentration of 35 mg/mL and kept in a freezer at −20 °C. On the day of the experiment, Infasurf was diluted to a final phospholipid concentration of 1 mg/mL using a saline buffer of 0.9% NaCl, 1.5 mM CaCl₂, and 2.5 mM HEPES, at pH 7.0.

Microplastics/Nanoplastics (MPs/NPs). MP samples were produced by following a protocol described previously.³³ Briefly, the preparation of MP samples from disposable lunch boxes made of polypropylene (lunch box-PP), foam packaging boxes made of polystyrene (foam box-PS), and drinking water bottles made of poly(ethylene terephthalate) (water bottle-PET) first involved cutting the bulk material into squares or cubes of approximately 1 cm per side. Next, the materials were transferred into a crusher (HATTIECS 924D, Zhongshan Huiren Electric, Guangdong, China) where they were treated with 50 mL/min liquid nitrogen to be thoroughly broken down into fine fragments. Finally, these plastic fragments were sieved into 100-200 µm particles and washed of impurities using deionized water and absolute ethanol. During the manufacturing process, incidentally formed NP debris was also collected without actively separating them from the larger MP fractions. The samples were stored in sealed containers until further use. The morphology and primary size of all MP/ NP samples were characterized with a Hitachi S-4800 field emission scanning electron microscope.

Animal Exposure and Analysis of Immune Cell Subtypes. The animal experiment protocols were approved by the Animal Ethics Committee at the Research Center for Eco-Environmental Sciences, Chinese Academy of Sciences (approval number: AEWC-RCEES-2020001). Specific pathogen-free (SPF) BALB/c mice (female, 6–7 weeks old) were obtained from Vital River Laboratory Animal Technology Co., Ltd. (Beijing, China), and were housed and maintained in an SPF facility. The mice were randomly divided into four groups (*n* = 4 per group), including one control group receiving only saline.

Mice in three exposure groups were intranasally administrated with 2 mg/kg dry powder of MP/NP per kg body weight, equivalent to 50 μ g for mice with 25 g weight. This

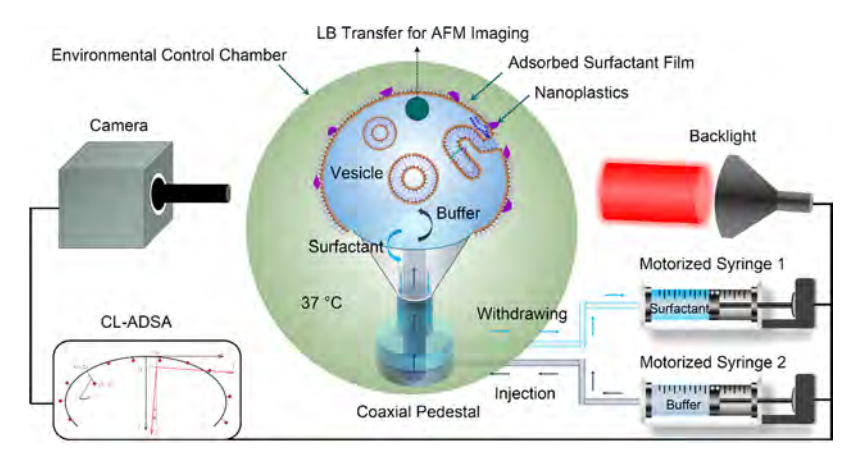


Figure 1. Schematic of constrained drop surfactometry (CDS). A pulmonary surfactant film is formed by adsorption to the air—water surface of a droplet, constrained on a 3 mm pedestal with knife-sharp edges and enclosed in an environmental control chamber maintained at 37 °C. Surface tension and surface area of the surfactant film are determined simultaneously from the shape of the droplet using closed-loop axisymmetric drop shape analysis (CL-ADSA). Subphase replacement is implemented with a coaxial pedestal connected to two motorized syringes, with one withdrawing the vesicle-containing subphase from the droplet and another one simultaneously injecting buffer into the droplet with the same volumetric rate. The adsorbed surfactant film is subsequently Langmuir—Blodgett (LB) transferred from the air—water surface to a freshly peeled mica substrate for atomic force microscopy (AFM) imaging.

dose was estimated based on an approximate equivalence to the human inhalation burden of airborne carbon nanomaterials. The MP/NP dose for inhalation/airway exposure is not yet established. Exposure doses up to 100 μ g MP/NP per mouse have been used in previous rodent exposure models.

After further feeding in the SPF facility for 48 h, the mice were anesthetized after intraperitoneal injection of 100 μ L of sodium pentobarbital at 0.01 g/mL. The exposed serum and the control serum were separated from heart blood by centrifugation. The interleukin-6 (IL-6) concentration in the mouse serum was detected with a Mouse IL-6 ELISA kit (NeoBioscience, Shenzhen, China).

For analysis of lung damage and inflammatory cell infiltration, lung tissues were collected and fixed in 4% paraformaldehyde overnight. The samples were then dehydrated with different concentrations of alcohol, rendered transparent in xylene, embedded in paraffin, cut in serial sections, and mounted on glass slides. After deparaffinization, the sections were rehydrated and stained with hematoxylin and eosin (H&E). Histological images were collected through Pannoramic 250 Flash III (3DHISTECH Ltd., Budapest, Hungary) and were analyzed with CaseViewer 2.3 software.

For the quantitative analysis of immune cells in the lung, single-cell suspensions of lung tissue were prepared by enzymatic digestion. Briefly, fresh lung parenchymal tissues were perfused and digested in 2 mL of DMEM (Gibco) containing DNase I (Solarbio, China), 100 U/mL penicillinstreptomycin (HyClone), and 0.5 mg/mL Liberase (Roche, Switzerland) for 30 min at 37 $^{\circ}$ C, and filtered through a 70 μ m cell strainer. After red blood cell lysis, the single-cell suspension of lung parenchymal tissues was washed twice by centrifugation at 100g for 3 min and resuspended in Hanks' Balanced Salt Solution (Sigma-Aldrich) with 2% fetal bovine serum. The cells were subjected to surface staining with a series of antibodies at 4 °C for 20 min, protected from light, and analyzed using an Attune NxT platform (Thermo Fisher Scientific). Detailed information about the fluorescent-dyeconjugated antibodies used in the flow cytometry analysis can be found in Table S1 in the Supporting Information.

Constrained Drop Surfactometry (CDS). The CDS is an advanced droplet-based tensiometry technique developed in our laboratory for studying the biophysical function of pulmonary surfactant. 40 Our previous studies have established the capacity of the CDS as a high-fidelity in vitro model to probe the biophysical mechanisms of nano-bio interactions at the pulmonary surfactant film, and its capacity as a new alternative method to quantitatively evaluate the acute respiratory toxicity of engineered nanomaterials and PM2.5. 34,41,42 As shown in Figure 1, the CDS uses a 3 mm pedestal with knife-sharp edges to constrain an aqueous sessile drop, thus minimizing film leakage from the air-water surface. Pulmonary surfactant at the phospholipid concentration of 1 mg/mL is adsorbed to the air-water surface of the droplet to form a surfactant film under equilibrium conditions. The surfactant film is then compressed and expanded periodically to simulate normal tidal breathing, by precisely regulating fluid flow into and out of the droplet using a motorized syringe. Surface tension and surface area of the droplet are determined instantaneously from the shape of the droplet using an in-lab developed closed-loop axisymmetric drop shape analysis (CL-ADSA) algorithm. 43 To mimic the intra-alveolar environment, the pedestal-droplet assembly is enclosed in an environmental control chamber where the temperature and relative humidity are controlled at 37 °C and 100%, respectively.

Specifically, MP/NP samples were added to the pulmonary surfactant suspension at final particle concentrations of 10, 100, and 1000 μ g/mL (or mg/L). These particle concentrations were selected to cover the wide concentration range (i.e., 0.05–1000 μ g/mL) previously used to assess the in vitro cytotoxicity of MPs, NPs, or polymeric micro/nanoparticles on human alveolar epithelial cells (such as A549)^{44,45} and human bronchial epithelial cells (such as BEAS-2B). The surfactant–plastic mixtures were incubated at 37 °C for 30 min and were vortexed for 10 s prior to CDS measurements. A droplet (~7 μ L) of the surfactant–plastic mixture was dispensed onto a 3 mm CDS pedestal. After rapid surfactant adsorption at the air—water surface, the surface tension decreased to an equilibrium value between 22 and 25 mN/m. The adsorbed surfactant film was then subject to dynamic cycling at a

Table 1. Characterization of the Morphology and Primary Size of Microplastics (MPs) and Incidentally Produced Nanoplastics (NPs)

MPs/NPs	Lunch box-PP	Foam box-PS	Water bottle-PET
Primary chemical composition	Polypropylene (PP) $(C_3H_6)_n$	Polystyrene (PS) $(C_8H_8)_n$	Polyethylene terephthalate (PET) (C ₁₀ H ₈ O ₄) _n
Chemical structure	CH ₃	M M M	H-OO-OO-OOH
MP morphology	100 µт	100 µm	100 µm
MP size (μm)	190 ± 26	180 ± 27	430 ± 92
NP morphology	₹ ₹ 1 1 1 1 1 1 1 1 1 1 1 1 1 1 1 1 1 1	t 200 nm	t t 2 mm
NP size (nm)	225 ± 68	52 ± 12	265 ± 109

physiologically relevant compression ratio of ~20% of the initial surface area, at a rate of 3 s per cycle to simulate normal tidal breathing. The minimum surface tension ($\gamma_{\rm min}$) and the film compressibility $\left(\kappa = \frac{1}{A} \frac{\partial A}{\partial \gamma}\right)$ of the 10th compression—expansion cycle were analyzed to quantify the biophysical properties of the surfactant film and the influence of the MP/NP samples.

Subphase Replacement and In Situ Langmuir-**Blodgett (LB) Transfer.** To facilitate visualization of the adsorbed surfactant film and nano-bio interactions using atomic force microscopy (AFM), we have developed a novel subphase replacement technique. 48 This technique is illustrated in Figure 1. Prior to in situ LB transfer from the droplet surface, the surfactant suspension was withdrawn from the droplet, while an equal amount of buffer was simultaneously injected into the droplet using a coaxial pedestal so that the volume of the droplet remained constant. Consequently, nonadsorbed phospholipid vesicles were washed out from the droplet without disturbing the adsorbed surfactant film at the air-water surface. After the subphase replacement, the adsorbed surfactant film at the air-water surface was LB transferred onto a freshly peeled mica surface by lifting it across the air-water surface at a rate of 1 mm/min.

Atomic Force Microscopy (AFM). An Innova AFM instrument (Bruker, Santa Barbara, CA) was used for imaging the topography of the adsorbed surfactant films. Using the tapping mode, the surfactant film with/without MP/NP samples was scanned in air using a silicon cantilever with a resonance frequency of 300 kHz and a spring constant of 42 mN/m. The reproducibility of the AFM imaging was ensured by scanning multiple samples at various locations. The AFM images were analyzed using Nanoscope Analysis (version 1.5). Multiple image analysis techniques were used. The height distribution of surfactant multilayers was estimated with bearing analysis, which provided information about the surface height histogram. The topographic profile of the heteroaggregated surfactant film was studied with section analysis.

The size distribution of NPs heteroaggregated with the surfactant film was studied with grain size analysis.

Statistical Analysis. Biophysical results were displayed as mean \pm standard deviation (n = 5). Group differences were determined through one-way ANOVA with the Tukey means comparison test (OriginPro, Northampton, MA). Results were considered statistically significant when p < 0.05.

RESULTS

Characterization of the MPs/NPs. Table 1 shows the primary chemical composition, morphology, and primary size of the MPs and incidentally produced NPs. Other physicochemical properties of these samples, such as their BET surface area, water contact angle, and zeta potential, have been thoroughly characterized and reported in a previous study.³³ The primary chemicals of these MP/NP samples increase their complexity from a linear hydrocarbon polymer (PP) to an aromatic hydrocarbon polymer (PS), and a condensation polymer of ethylene glycol and terephthalic acid (PET). 49 All MP samples demonstrate a heterogeneous size distribution (ultrastructures of these MPs at lower magnifications can be found in Figure S1). The MPs are irregularly shaped with the lunch box-PP having an irregular blocklike structure, while the foam box-PS and the water bottle-PET have a crinkled flocculent morphology; albeit the latter is significantly larger. Incidentally produced NPs were found to coexist with all three MP samples. The NPs of lunch box-PP and water bottle-PET are all larger than 200 nm, while the NPs of foam box-PS are much smaller, around 52 nm. It was also found that the NPs of water bottle-PET tend to adhere to the surfaces of the MPs, while the NPs of the other two samples appear to be more isolated from their MP counterparts.

Biophysical Impact of MPs/NPs on Pulmonary Surfactant. Figure 2 shows the biophysical impacts of MPs/NPs at 10, 100, and 1000 μ g/mL (or mg/L), respectively, on Infasurf, a natural surfactant preparation derived from calf lungs. As shown in Figure 2, exposure to all three MP/NP samples at all three concentrations significantly increases the

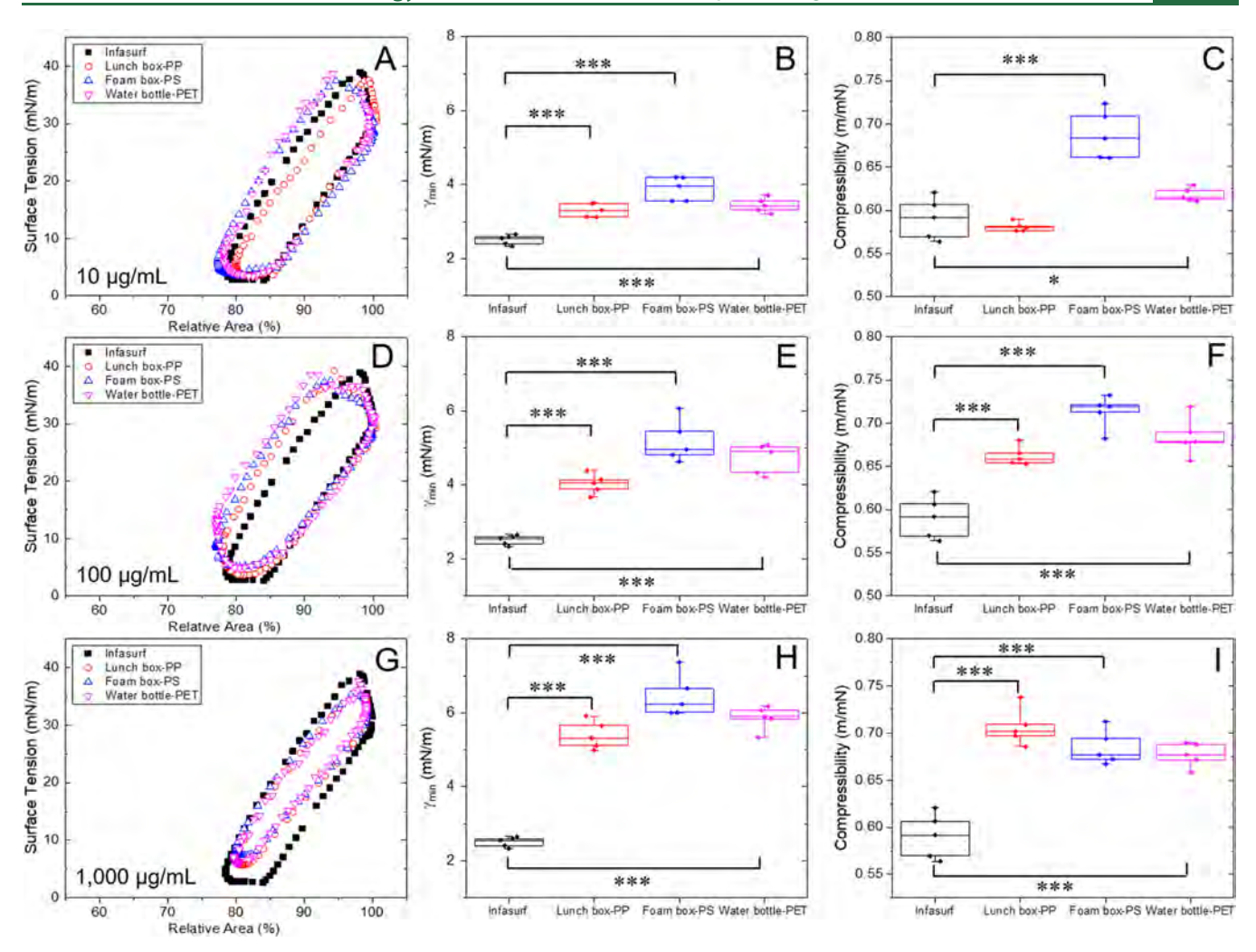


Figure 2. Biophysical impact of MPs/NPs at 10 μ g/mL (A–C), 100 μ g/mL (D–F), and 1000 μ g/mL (G–I), respectively, on the pulmonary surfactant. (A, D, G) Typical dynamic compression–expansion cycles, i.e., simulation of normal tidal breathing, with/without the MP/NP samples. (B, E, H) Statistical analysis of the minimum surface tensions (γ_{min}). (C, F, I) Statistical analysis of the film compressibility (κ). *p < 0.05, **p < 0.01, and ***p < 0.001.

minimum surface tension (γ_{min}) of Infasurf at the end of compression. For all three MP/NP samples, γ_{min} of Infasurf increases as a function of the MP/NP concentration. Specifically, at 10 $\mu g/mL$, the γ_{min} of Infasurf increases from 2.5 to 3.4, 3.9, and 3.5 mN/m when exposed to lunch box-PP, foam box-PS, and water bottle-PET, respectively. At 100 μ g/ mL, γ_{min} increases to 4.0, 5.2, and 4.7 mN/m upon exposure to these three MP/NP samples. At 1000 $\mu g/mL$, γ_{min} further increases to 5.4, 6.5, and 5.9 mN/m when exposed to lunch box-PP, foam box-PS, and water bottle-PET, respectively. The compressibility (κ) of the surfactant film also increased after exposure to all three MP/NP samples. The κ is a measure of film "hardness", with a higher κ indicating a "softer", more compressible film.²⁵ A surfactant film with a higher compressibility means that it requires a greater reduction in surface area to achieve low surface tensions, thus indicating surfactant inhibition. These data therefore indicate that exposure to MPs/NPs inhibited the biophysical function of the pulmonary surfactant. Furthermore, these in vitro data predict that the lung toxicity of the three MP/NP samples tested here can be roughly ranked as foam box-PS > water bottle-PET > lunch box-PP.

MP/NP-Induced Proinflammatory Responses and Lung Injury in Mice. Figure 3 shows the proinflammatory responses and lung injury caused by intranasal exposure of dry powder of these MP/NP samples at 2 mg/kg of body weight of mice. As illustrated in Figure 3A, we determined the MP/NP-induced proinflammatory responses and lung injury by studying the systemic cytokine, flow cytometry analysis of inflammatory cell subtypes in the single-cell suspension of lung tissue, and lung histology. Detailed flow cytometry analysis of the lung inflammatory cells can be found in Figure S2.

We found a significant increase of the IL-6 content, a classic proinflammatory cytokine, in the sera of MP/NP-treated mice (p < 0.001). In comparison to mice in the control group, the IL-6 content increases by 4.8-fold, 7.8-fold, and 6.0-fold for mice exposed to MPs/NPs derived from the lunch box-PP, foam box-PS, and water bottle-PET, respectively (Figure 3B). The white blood cells (CD45⁺) in the lung of mice exposed to foam box-PS increase by 24% (p < 0.05), in comparison to the control group (Figure 3C). The inflammatory cell subtypes mainly consist of macrophages, neutrophils, eosinophils, monocytes, and dendritic cells (DCs) (Figure S2). It was found that among all three MP/NP samples, exposure to MP/NP derived from the foam box-PS caused the largest increase

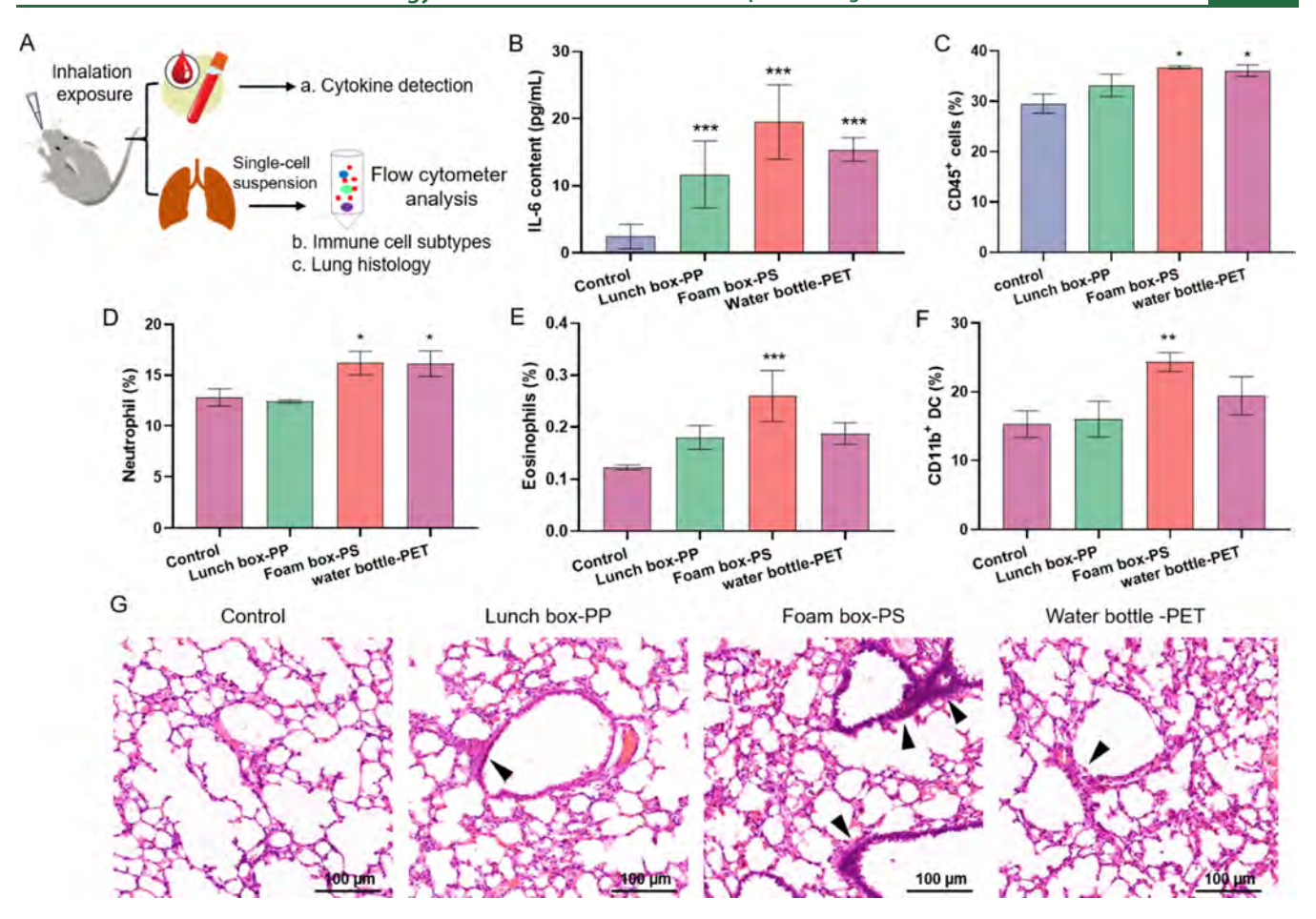


Figure 3. Proinflammatory response and lung damage caused by exposure to aspirated dry powder of MP/NP samples at 2 mg/kg of body weight of mice. (A) Schematic procedures for assessing the MP/NP-induced inflammatory lung damage by studying systemic cytokines, immune cell subtypes, and lung histology. (B) ELISA assay of the IL-6 content in sera from mice treated with various MP/NP samples. (C) Flow cytometry analysis of the percentage of CD45⁺ white blood cells in the lung tissue. (D–F) Percentage of the immune cell subtypes, including neutrophil (CD45⁺CD11b⁺CD170⁻Ly6G⁺) (D), eosinophils (CD45⁺CD11b[±]CD170⁺Ly6G⁻CD11c⁻) (E), and CD11b⁺ dendritic cells (CD45⁺Ly6G⁻CD11b[±]CD24⁺CD11c⁺MHCII⁺) (F). (G) H&E-stained lung sections from mice exposed to various MP/NP samples for 48 h. Infiltration of inflammatory cells is indicated by black arrows; *p < 0.05; ***p < 0.01; ***p < 0.001.

of the inflammatory cell subtypes in the lung. Compared to the control group, neutrophil, eosinophil, and CD11b⁺ DCs in the lung tissue of mice exposed to the foam box-PS increase by 26.5% (Figure 3D, p < 0.05), 1.1-fold (Figure 3E, p < 0.001), and 59.4% (Figure 3F, p < 0.01), respectively. Furthermore, infiltration of inflammatory cells and lung damage are visualized by the H&E-stained lung tissues (Figure 3G). Together, these in vivo data suggest that the lung toxicity of the three MP/NP samples tested here is ranked as foam box-PS > water bottle-PET > lunch box-PP, in good agreement with the ranking predicted by the in vitro biophysical simulations (Figure 2).

Effect of MPs/NPs on the Ultrastructure and Topography of the Pulmonary Surfactant Film. To study the mechanism of MP/NP-induced surfactant inhibition and the corresponding lung toxicity, Figure 4 shows the AFM topographic images of the Infasurf film with/without exposure to MP/NP samples at $1000~\mu g/mL$. It should be noted that to obtain high-contrast AFM images, a high particle concentration of $1000~\mu g/mL$ was used to augment the MP/NP-induced alterations to the ultrastructure and topography of the surfactant film. A more environmentally relevant low particle concentration of $10~\mu g/mL$ caused qualitatively similar alterations to the surfactant film (see Figure S3 for details).

Moreover, the purpose of the AFM imaging is not to detect MPs, if any, adsorbed to the Infasurf film, since its maximum field of view (100 μ m × 100 μ m) is less than the primary size of these MPs (Table 1). Rather, AFM imaging was used to probe the potential adsorption and heteroaggregation of the incidentally formed NPs, coexisting with the MPs as shown in Table 1.

As shown in Figure 4A, the adsorbed Infasurf film without exposure to MPs/NPs shows uniformly distributed phospholipid multilayers, with a maximum height up to 40 nm (Figure 4E), throughout the surfactant film. Bearing analysis of the AFM images shows that the mean height of these multilayer structures is 22 nm, corresponding to 5-6 stacked phospholipid bilayers (Figure 4I), given the thickness of fully hydrated phospholipid bilayers to be ~4 nm. 50 After exposure to MPs/NPs, the lateral structure and topography of the Infasurf film are significantly altered. As shown in Figure 4B, after exposure to lunch box-PP, the ultrastructure shows isolated large aggregates sparsely scattered in the Infasurf film. The height profile of such an aggregate is shown in Figure 4J. The peak height of this aggregate is up to 56 nm, and its height profile is completely different from that of stacked bilayers in phospholipid multilayers, 48 thus indicating that this large

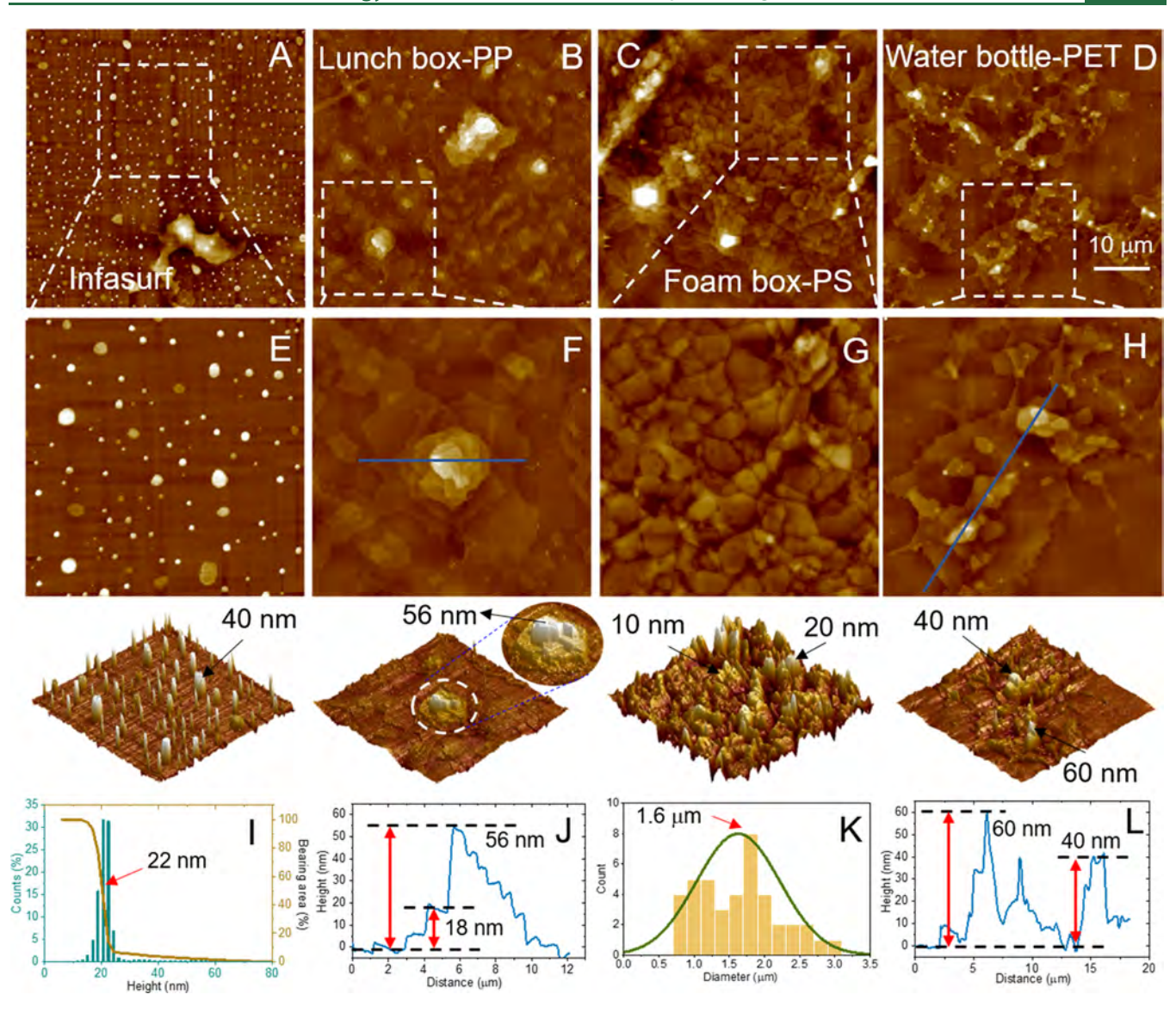


Figure 4. Effect of MPs/NPs (1000 μ g/mL) on the ultrastructure and topography of the pulmonary surfactant film. (A) AFM image of a de novo adsorbed Infasurf film. (B–D) AFM images of the adsorbed Infasurf film after exposure to lunch box-PP (B), foam box-PS (C), and water bottle-PET (D), respectively. All AFM images shown in (A–D) have the same scanning area of 50 μ m × 50 μ m. (E–H) Close-up images indicated by the white boxes in (A–D). Images in the third row show the 3D rendering of the close-up images shown in (E–H). Detailed multilayer structures are shown in circles. Single-headed black arrows indicate the heights of structures. The z range for all of the images is 100 nm. (I–L) Bearing analysis, height histogram, and grain size analysis of structures shown in (E–H).

aggregate most likely represents NPs heteroaggregated with the surfactant film.

When Infasurf is exposed to foam box-PS (Figure 4C), the entire surfactant film is monopolized with grainlike structures with an average diameter of 1.6 μ m (Figure 4K) and a relative height contrast between 10 and 20 nm. These structures appear to be the incidentally formed foam box-PS NPs, adsorbed to and heteroaggregated with the Infasurf film. When Infasurf is exposed to water bottle-PET (Figure 4D), the ultrastructure exhibits a few irregularly shaped large structures, up to 60 nm in height (Figure 4L), corresponding to water bottle-PET NPs adsorbed to and heteroaggregated with the Infasurf film.

DISCUSSION

Among all three MP/NP samples, the foam box-PS demonstrated the highest adverse impact on the biophysical

properties of pulmonary surfactant (Figure 2), and it also caused the largest inflammatory responses and lung injury (Figure 3). The deleterious effects on surfactant biophysics are revealed by a significant increase in the minimum surface tension (γ_{\min}) and compressibility (κ) of the surfactant film (Figure 2). Both γ_{min} and κ are the gold standard for evaluating the biophysical function of pulmonary surfactant film. 25,41 A good surfactant film should be able to decrease the alveolar surface tension down to near-zero values with only a moderate compression (<20% area reduction), i.e., having a very low compressibility close to that of a pure dipalmitoylphosphatidylcholine (DPPC) monolayer.²⁵ Our recent study suggested that the natural pulmonary surfactant achieves this optimal biophysical function by forming an ordered DPPC monolayer immediately after adsorption, and thus no further compositional purification is needed during the subsequent film compression-expansion cycles.⁴⁸ Increasing γ_{min} and κ in the

case of surfactant inhibition are associated with an increased effort for breathing, which is the condition of various respiratory diseases such as the respiratory distress syndrome and acute lung injury. Additionally, it was recently found that the increase in surface tension resulting from surfactant inhibition due to exposure to polyhexamethylene guanidine, a common disinfectant used in household humidifiers, may contribute to pulmonary fibrosis. 1

Engineered nanomaterials (ENMs), especially polystyrene (PS) nanoparticles, are commonly used for studying nano-bio interactions and the EHS impact of ENMs. 52-54 This is in part due to the well-controlled physicochemical properties of engineered PS nanoparticles/nanospheres. It was found that engineered PS nanoparticles caused substantially more pulmonary toxicological effects than other polymeric nanoparticles,⁵² likely due to their high surface hydrophobicity that promotes the production of more reactive oxygen species (ROS) and lung inflammation.⁵³ Our previous study also showed that engineered PS nanoparticles demonstrated more inhibitory effects than other polymeric nanoparticles on the biophysical properties of pulmonary surfactant.⁵⁴ The PS nanoparticles were found to directly interact with natural surfactant films, thus adsorbing surfactant phospholipids and proteins to form the so-called pulmonary surfactant biomolecular corona. 55,56 Once adsorbed to the nanoparticle surfaces, the hydrophobic surfactant proteins (SP-B/C) undergo denaturation, thus leading to surfactant inactivation.⁵

MPs/NPs differ from ENMs in the heterogeneity and irregularity of their morphology and composition. ¹⁴ While most engineered PS nanoparticles are monodispersed nanospheres, MP/NP derived from the foam box-PS demonstrated significant heterogeneity in size with coexisting MPs and NPs, and with shapes of high aspect ratios (Table 1). These morphological differences between MPs/NPs and ENMs may have a profound impact on their interaction behavior with biomembranes and even their endocytosis pathways. Fleury and Baulinc have shown that the heterogeneity of MPs in shape and morphology appears to be an important risk factor for their interaction potential with cell membranes.²⁹ It was found that MPs adsorbed to biomembranes reduced the membrane area and increased the membrane tension, thus leading to reduced membrane lifetime.²⁹ The detailed interaction mechanism between the irregularly shaped MPs/ NPs and biomembranes may be similar to that revealed by Shi et al. ⁵⁸ These researchers found that in comparison to regularly shaped spherical and elliptical ENMs, nanomaterials with higher aspect ratios, such as carbon nanotubes, may interact with cell membranes via tip recognition, followed by rotation of the nanomaterials.⁵⁸ Similar shape-dependent mechanisms were also proposed to explain interactions between nanomaterials with higher aspect ratios and simulated pulmonary surfactant monolayers.

Using AFM, we directly visualized the adsorption of NPs to the pulmonary surfactant film. NPs are incidentally produced debris from the environmental fragmentation of MPs. Due to their small colloidal size, and hence large surface area-to-volume ratio, NPs are expected to have a high bioavailability and thus readily heteroaggregate with biomolecules or other environmental macromolecules. Although the incidentally formed NPs only make up a small mass fraction of the MP-NP-biomolecular heteroaggregates, the NPs likely play a predominant role in determining the nano-bio interactions and hence toxicity of the MPs/NPs complex. Compared to

lunch box-PP and water bottle-PET, it was found that NPs of foam box-PS almost completely monopolized the air-water surface and heteroaggregated with the pulmonary surfactant film (Figure 4). Such a heteroaggregation state at the surface is in good agreement with in vitro biophysical inhibition (Figure 2) and in vivo inflammatory responses (Figure 3) caused by the foam box-PS. This is most likely related to the much smaller size of the NPs derived from the foam box-PS (Table 1), which leads to more adsorption and heteroaggregation with surfactant phospholipids and proteins. We tested this hypothesis indirectly by measuring the phospholipid vesicle sizes with/without MPs/NPs using dynamic light scattering (Zetasizer, Malvern). It was found that the addition of MPs/ NPs significantly decreases the vesicle size of Infasurf (Figure S4). This indicates denaturation of surfactant-associated proteins (SP-B/C), since these small, hydrophobic proteins promote the formation of large vesicular aggregates by inducing membrane fusion. 57,60 Decreasing phospholipid vesicle size in natural pulmonary surfactants is a strong indication of surfactant inhibition. Figure 5 depicts the main findings and the EHS impact of this study.

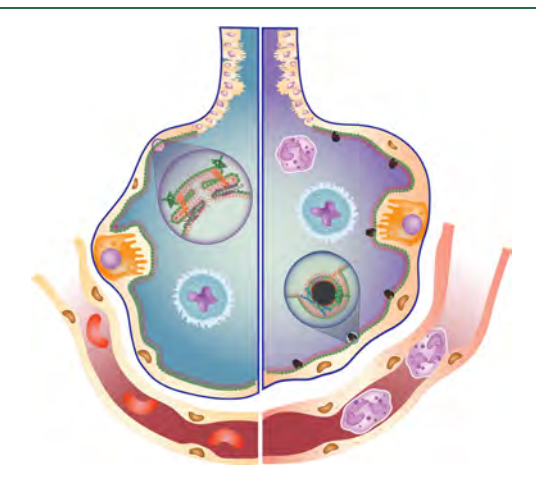


Figure 5. Schematic illustration of micro/nanoplastic-induced lung injury. The left-half of the schematic shows a normal alveolus. The pulmonary surfactant, synthesized by the alveolar type II epithelial cells, covers the entire air—water surface of the alveolus, in the form of a multilayered phospholipid film stabilized by surfactant-associated proteins. The right-half of the schematic shows the injured alveolus due to particulate insults. Alveolar macrophages secrete cytokines, such as interleukin (IL)-6. Immune cells, such as neutrophils, eosinophils (not shown), and dendritic cells (not shown), are recruited to the alveolar space. Nanoplastics form heteroaggregation with the pulmonary surfactant film at the alveolar—capillary interface, thus inhibiting the biophysical function of pulmonary surfactant.

In conclusion, we have studied the biophysical impacts of microplastics (MPs) and nanoplastics (NPs) derived from commonly used commercial plastic products on a natural pulmonary surfactant extracted from calf lung lavage using constrained drop surfactometry (CDS). It was found that in comparison to MPs/NPs derived from disposable lunch boxes made of polypropylene (lunch box-PP) or from drinking water bottles made of poly(ethylene terephthalate) (water bottle-PET), the MP/NP derived from foam packaging boxes made of polystyrene (foam box-PS) showed the highest adverse impact on the biophysical properties of pulmonary surfactant and also caused the most serious proinflammatory responses and lung injury in mice. Atomic force microscopy (AFM)

revealed that all three NP samples were adsorbed to the air—water surface and heteroaggregated with the pulmonary surfactant film, with foam box-PS almost completely monopolizing the surfactant film. These results indicate that although the incidentally formed NPs only make up a small mass fraction of the MP-NP-biomolecular heteroaggregates, they likely play a predominant role in determining the nanobio interactions and hence toxicity of the MPs/NPs complex. These findings may provide novel insights into understanding the health impact of MPs and NPs on the respiratory system.

ASSOCIATED CONTENT

Supporting Information

The Supporting Information is available free of charge at https://pubs.acs.org/doi/10.1021/acs.est.3c06668.

Additional experimental results; fluorescent-dye-conjugated antibodies used in the flow cytometry analysis; electron microscopy images of the MP samples; flow cytometry analysis of immune cell subtypes; AFM images of NP heteroaggregation with the pulmonary surfactant film; and dynamic light scattering analysis of phospholipid vesicle sizes with/without MP/NP samples (PDF)

AUTHOR INFORMATION

Corresponding Authors

Juan Ma – State Key Laboratory of Environmental Chemistry and Ecotoxicology, Research Center for Eco-Environmental Sciences, Chinese Academy of Sciences, Beijing 100085, P. R. China; College of Resources and Environment, University of Chinese Academy of Sciences, Beijing 101314, P. R. China; Phone: 010-62849050; Email: juanm@rcees.ac.cn

Yi Y. Zuo — Department of Mechanical Engineering, University of Hawaii at Manoa, Honolulu, Hawaii 96822, United States; Department of Pediatrics, John A. Burns School of Medicine, University of Hawaii, Honolulu, Hawaii 96826, United States; orcid.org/0000-0002-3992-3238; Phone: 808-956-9650; Email: yzuo@hawaii.edu; Fax: 808-956-2373

Authors

Xiaojie Xu — Department of Mechanical Engineering, University of Hawaii at Manoa, Honolulu, Hawaii 96822, United States

Ria A. Goros – Department of Mechanical Engineering, University of Hawaii at Manoa, Honolulu, Hawaii 96822, United States

Zheng Dong — State Key Laboratory of Environmental Chemistry and Ecotoxicology, Research Center for Eco-Environmental Sciences, Chinese Academy of Sciences, Beijing 100085, P. R. China; College of Resources and Environment, University of Chinese Academy of Sciences, Beijing 101314, P. R. China; Medical Science and Technology Innovation Center, Shandong First Medical University & Shandong Academy of Medical Sciences, Jinan 250117 Shandong, P. R.

Xin Meng — College of Environmental Science and Engineering, Ministry of Education Key Laboratory of Pollution Processes and Environmental Criteria, Tianjin Key Laboratory of Environmental Remediation and Pollution Control, Nankai University, Tianjin 300350, P. R. China Guangle Li — Department of Mechanical Engineering, University of Hawaii at Manoa, Honolulu, Hawaii 96822, United States

Wei Chen — College of Environmental Science and Engineering, Ministry of Education Key Laboratory of Pollution Processes and Environmental Criteria, Tianjin Key Laboratory of Environmental Remediation and Pollution Control, Nankai University, Tianjin 300350, P. R. China; orcid.org/0000-0003-2106-4284

Sijin Liu – State Key Laboratory of Environmental Chemistry and Ecotoxicology, Research Center for Eco-Environmental Sciences, Chinese Academy of Sciences, Beijing 100085, P. R. China; College of Resources and Environment, University of Chinese Academy of Sciences, Beijing 101314, P. R. China; Medical Science and Technology Innovation Center, Shandong First Medical University & Shandong Academy of Medical Sciences, Jinan 250117 Shandong, P. R. China; orcid.org/0000-0002-5643-0734

Complete contact information is available at: https://pubs.acs.org/10.1021/acs.est.3c06668

Author Contributions

 ${}^{
abla}\! X.X.$ and R.A.G. contributed equally to this work.

Notes

The authors declare no competing financial interest.

ACKNOWLEDGMENTS

The authors thank Dr. Sindhu Row of ONY Biotech for donation of Infasurf samples. This work was supported by the National Science Foundation (grant number CBET-2011317) to Y.Y.Z., the Youth Innovation Promotion Association of Chinese Academy of Science (2022042) to J.M., and an International Collaboration Key Grant from the Chinese Academy of Sciences (grant number 121311KYSB20190010) to S.J.L.

■ REFERENCES

- (1) Hartmann, N. B.; Huffer, T.; Thompson, R. C.; Hassellov, M.; Verschoor, A.; Daugaard, A. E.; Rist, S.; Karlsson, T.; Brennholt, N.; Cole, M.; Herrling, M. P.; Hess, M. C.; Ivleva, N. P.; Lusher, A. L.; Wagner, M. Are We Speaking the Same Language? Recommendations for a Definition and Categorization Framework for Plastic Debris. *Environ. Sci. Technol.* **2019**, *53* (3), 1039–1047.
- (2) Vethaak, A. D.; Legler, J. Microplastics and human health. *Science* **2021**, *371* (6530), 672–674.
- (3) Kubowicz, S.; Booth, A. M. Biodegradability of Plastics: Challenges and Misconceptions. *Environ. Sci. Technol.* **2017**, *51* (21), 12058–12060.
- (4) Mao, R.; Lang, M.; Yu, X.; Wu, R.; Yang, X.; Guo, X. Aging mechanism of microplastics with UV irradiation and its effects on the adsorption of heavy metals. *J. Hazard. Mater.* **2020**, 393, No. 122515.
- (5) Zhang, K.; Hamidian, A. H.; Tubic, A.; Zhang, Y.; Fang, J. K. H.; Wu, C.; Lam, P. K. S. Understanding plastic degradation and microplastic formation in the environment: A review. *Environ. Pollut.* **2021**, *274*, No. 116554.
- (6) Rillig, M. C. Microplastic in terrestrial ecosystems and the soil? *Environ. Sci. Technol.* **2012**, 46 (12), 6453–6454.
- (7) Browne, M. A.; Crump, P.; Niven, S. J.; Teuten, E.; Tonkin, A.; Galloway, T.; Thompson, R. Accumulation of Microplastic on Shorelines Woldwide: Sources and Sinks. *Environ. Sci. Technol.* **2011**, 45 (21), 9175–9179.
- (8) Alimi, O. S.; Budarz, J. F.; Hernandez, L. M.; Tufenkji, N. Microplastics and Nanoplastics in Aquatic Environments: Aggregation, Deposition, and Enhanced Contaminant Transport. *Environ. Sci. Technol.* **2018**, 52 (4), 1704–1724.

- (9) Wright, S. L.; Thompson, R. C.; Galloway, T. S. The physical impacts of microplastics on marine organisms: a review. *Environ. Pollut.* **2013**, *178*, 483–492.
- (10) Amato-Lourenco, L. F.; Dos Santos Galvao, L.; de Weger, L. A.; Hiemstra, P. S.; Vijver, M. G.; Mauad, T. An emerging class of air pollutants: Potential effects of microplastics to respiratory human health? *Sci. Total Environ.* **2020**, *749*, No. 141676.
- (11) Prata, J. C. Airborne microplastics: Consequences to human health? *Environ. Pollut.* **2018**, 234, 115–126.
- (12) Pizarro-Ortega, C. I.; Dioses-Salinas, D. C.; Severini, M. D. F.; Lopez, A. D. F.; Rimondino, G. N.; Benson, N. U.; Dobaradaran, S.; De-la-Torre, G. E. Degradation of plastics associated with the COVID-19 pandemic. *Mar. Pollut. Bull.* **2022**, *176*, No. 113474.
- (13) Ivleva, N. P. Chemical Analysis of Microplastics and Nanoplastics: Challenges, Advanced Methods, and Perspectives. *Chem. Rev.* **2021**, *121* (19), 11886–11936.
- (14) Gigault, J.; El Hadri, H.; Nguyen, B.; Grassl, B.; Rowenczyk, L.; Tufenkji, N.; Feng, S.; Wiesner, M. Nanoplastics are neither microplastics nor engineered nanoparticles. *Nat. Nanotechnol.* **2021**, *16* (5), 501–507.
- (15) Cox, K. D.; Covernton, G. A.; Davies, H. L.; Dower, J. F.; Juanes, F.; Dudas, S. E. Human Consumption of Microplastics. *Environ. Sci. Technol.* **2019**, *53* (12), 7068–7074.
- (16) Jenner, L. C.; Rotchell, J. M.; Bennett, R. T.; Cowen, M.; Tentzeris, V.; Sadofsky, L. R. Detection of microplastics in human lung tissue using μ FTIR spectroscopy. *Sci. Total Environ.* **2022**, 831, No. 154907.
- (17) Amato-Lourenço, L. F.; Carvalho-Oliveira, R.; Júnior, G. R.; dos Santos Galvão, L.; Ando, R. A.; Mauad, T. Presence of airborne microplastics in human lung tissue. *J. Hazard. Mater.* **2021**, *416*, No. 126124.
- (18) Dris, R.; Gasperi, J.; Saad, M.; Mirande, C.; Tassin, B. Synthetic fibers in atmospheric fallout: A source of microplastics in the environment? *Mar. Pollut. Bull.* **2016**, *104* (1–2), 290–293.
- (19) Wright, S. L.; Kelly, F. J. Plastic and Human Health: A Micro Issue? *Environ. Sci. Technol.* **2017**, *51* (12), 6634–6647.
- (20) Dewika, M.; Markandan, K.; Irfan, N. A.; Abdah, M. A. A. M.; Ruwaida, J. N.; Sara, Y. Y.; Khalid, M. Review of microplastics in the indoor environment: Distribution, human exposure and potential health impacts. *Chemosphere* **2023**, *324*, No. 138270.
- (21) O'Brien, S.; Rauert, C.; Ribeiro, F.; Okoffo, E. D.; Burrows, S. D.; O'Brien, J. W.; Wang, X.; Wright, S. L.; Thomas, K. V. There's something in the air: A review of sources, prevalence and behaviour of microplastics in the atmosphere. *Sci. Total Environ.* **2023**, 874, No. 162193.
- (22) Zuo, Y. Y.; Uspal, W. E.; Wei, T. Airborne Transmission of COVID-19: Aerosol Dispersion, Lung Deposition, and Virus-Receptor Interactions. ACS Nano 2020, 14 (12), 16502–16524.
- (23) Ruge, C. A.; Kirch, J.; Lehr, C.-M. Pulmonary drug delivery: from generating aerosols to overcoming biological barriers—therapeutic possibilities and technological challenges. *Lancet Respir. Med.* **2013**, *1* (5), 402–413.
- (24) Li, Y.; Shi, T.; Li, X.; Sun, H.; Xia, X.; Ji, X.; Zhang, J.; Liu, M.; Lin, Y.; Zhang, R.; Zheng, Y.; Tang, J. Inhaled tire-wear microplastic particles induced pulmonary fibrotic injury via epithelial cytoskeleton rearrangement. *Environ. Int.* **2022**, *164*, No. 107257.
- (25) Zuo, Y. Y.; Veldhuizen, R. A.; Neumann, A. W.; Petersen, N. O.; Possmayer, F. Current perspectives in pulmonary surfactant—inhibition, enhancement and evaluation. *Biochim. Biophys. Acta, Biomembr.* **2008**, *1778* (10), 1947–1977.
- (26) Garcia-Mouton, C.; Hidalgo, A.; Cruz, A.; Pérez-Gil, J. The Lord of the Lungs: The essential role of pulmonary surfactant upon inhalation of nanoparticles. *Eur. J. Pharm. Biopharm.* **2019**, *144*, 230–243
- (27) Li, L.; Xu, Y.; Li, S.; Zhang, X.; Feng, H.; Dai, Y.; Zhao, J.; Yue, T. Molecular modeling of nanoplastic transformations in alveolar fluid and impacts on the lung surfactant film. *J. Hazard. Mater.* **2022**, 427, No. 127872.

- (28) Shi, W.; Cao, Y.; Chai, X.; Zhao, Q.; Geng, Y.; Liu, D.; Tian, S. Potential health risks of the interaction of microplastics and lung surfactant. *J. Hazard. Mater.* **2022**, 429, No. 128109.
- (29) Fleury, J. B.; Baulin, V. A. Microplastics destabilize lipid membranes by mechanical stretching. *Proc. Natl. Acad. Sci. U.S.A.* **2021**, *118* (31), No. e2104610118, DOI: 10.1073/pnas.2104610118.
- (30) Danopoulos, E.; Twiddy, M.; West, R.; Rotchell, J. M. A rapid review and meta-regression analyses of the toxicological impacts of microplastic exposure in human cells. *J. Hazard. Mater.* **2022**, 427, No. 127861.
- (31) Zhang, H.; Fan, Q.; Wang, Y. E.; Neal, C. R.; Zuo, Y. Y. Comparative study of clinical pulmonary surfactants using atomic force microscopy. *Biochim. Biophys. Acta, Biomembr.* **2011**, *1808* (7), 1832–1842.
- (32) Postle, A. D.; Heeley, E. L.; Wilton, D. C. A comparison of the molecular species compositions of mammalian lung surfactant phospholipids. *Comp. Biochem. Physiol., Part A: Mol. Integr. Physiol.* **2001**, *129* (1), 65–73.
- (33) Duan, L.; Qin, Y.; Meng, X.; Liu, Y.; Zhang, T.; Chen, W. Sulfide- and UV-induced aging differentially affect contaminant-binding properties of microplastics derived from commercial plastic products. *Sci. Total Environ.* **2023**, *869*, No. 161800.
- (34) Valle, R. P.; Wu, T.; Zuo, Y. Y. Biophysical influence of airborne carbon nanomaterials on natural pulmonary surfactant. *ACS Nano* **2015**, *9* (5), 5413–5421.
- (35) NIOSH, US. Current Intelligence Bulletin 65: Occupational Exposure to Carbon Nanotubes and Nanofibers; NIOSH: Cincinnati, OH, USA, 2013 https://www.cdc.gov/niosh/docs/2013-145/default.html (accessed November 3, 2023).
- (36) da Silva Brito, W. A.; Mutter, F.; Wende, K.; Cecchini, A. L.; Schmidt, A.; Bekeschus, S. Consequences of nano and microplastic exposure in rodent models: the known and unknown. *Part. Fibre Toxicol.* **2022**, *19* (1), No. 28, DOI: 10.1186/s12989-022-00473-y.
- (37) Sun, A.; Wang, W.-X. Human Exposure to Microplastics and Its Associated Health Risks. *Environ. Health* **2023**, *1* (3), 139–149.
- (38) Lim, D.; Jeong, J.; Song, K. S.; Sung, J. H.; Oh, S. M.; Choi, J. Inhalation toxicity of polystyrene micro(nano)plastics using modified OECD TG 412. *Chemosphere* **2021**, 262, No. 128330.
- (39) Zha, H.; Xia, J.; Li, S.; Lv, J.; Zhuge, A.; Tang, R.; Wang, S.; Wang, K.; Chang, K.; Li, L. Airborne polystyrene microplastics and nanoplastics induce nasal and lung microbial dysbiosis in mice. *Chemosphere* **2023**, *310*, No. 136764.
- (40) Xu, X.; Li, G.; Zuo, Y. Y. Constrained drop surfactometry for studying adsorbed pulmonary surfactant at physiologically relevant high concentrations. *Am. J. Physiol.: Lung Cell. Mol. Physiol.* **2023**, 325 (4), L508–L517.
- (41) Yang, Y.; Xu, L.; Dekkers, S.; Zhang, L. G.; Cassee, F. R.; Zuo, Y. Y. Aggregation State of Metal-Based Nanomaterials at the Pulmonary Surfactant Film Determines Biophysical Inhibition. *Environ. Sci. Technol.* **2018**, *52* (15), 8920–8929.
- (42) Yang, Y.; Wu, Y.; Ren, Q.; Zhang, L. G.; Liu, S.; Zuo, Y. Y. Biophysical Assessment of Pulmonary Surfactant Predicts the Lung Toxicity of Nanomaterials. *Small Methods* **2018**, 2 (4), No. 1700367, DOI: 10.1002/smtd.201700367.
- (43) Yu, K.; Yang, J.; Zuo, Y. Y. Automated Droplet Manipulation Using Closed-Loop Axisymmetric Drop Shape Analysis. *Langmuir* **2016**, 32 (19), 4820–4826.
- (44) Goodman, K. E.; Hare, J. T.; Khamis, Z. I.; Hua, T.; Sang, Q. A. Exposure of Human Lung Cells to Polystyrene Microplastics Significantly Retards Cell Proliferation and Triggers Morphological Changes. *Chem. Res. Toxicol.* **2021**, *34* (4), 1069–1081.
- (45) Shi, Q.; Tang, J.; Wang, L.; Liu, R.; Giesy, J. P. Combined cytotoxicity of polystyrene nanoplastics and phthalate esters on human lung epithelial A549 cells and its mechanism. *Ecotoxicol. Environ. Saf.* **2021**, 213, No. 112041.
- (46) Yang, S.; Cheng, Y.; Chen, Z.; Liu, T.; Yin, L.; Pu, Y.; Liang, G. In vitro evaluation of nanoplastics using human lung epithelial cells, microarray analysis and co-culture model. *Ecotoxicol. Environ. Saf.* **2021**, 226, No. 112837.

- (47) Bachofen, H.; Schurch, S.; Urbinelli, M.; Weibel, E. R. Relations among alveolar surface tension, surface area, volume, and recoil pressure. *J. Appl. Physiol.* **1987**, *62* (5), 1878–1887.
- (48) Xu, L.; Yang, Y.; Zuo, Y. Y. Atomic Force Microscopy Imaging of Adsorbed Pulmonary Surfactant Films. *Biophys. J.* **2020**, *119* (4), 756–766.
- (49) Wang, Y.; Yang, Y.; Liu, X.; Zhao, J.; Liu, R.; Xing, B. Interaction of Microplastics with Antibiotics in Aquatic Environment: Distribution, Adsorption, and Toxicity. *Environ. Sci. Technol.* **2021**, *55* (23), 15579–15595.
- (50) Marsh, D. Handbook of Lipid Bilayers, 2nd ed.; CRC Press: Boca Raton, 2013.
- (51) Li, X.; Zhang, J.; Du, C.; Jiang, Y.; Zhang, W.; Wang, S.; Zhu, X.; Gao, J.; Zhang, X.; Ren, D.; Zheng, Y.; Tang, J. Polyhexamethylene guanidine aerosol triggers pulmonary fibrosis concomitant with elevated surface tension via inhibiting pulmonary surfactant. *J. Hazard. Mater.* **2021**, 420, No. 126642.
- (52) Dailey, L. A.; Jekel, N.; Fink, L.; Gessler, T.; Schmehl, T.; Wittmar, M.; Kissel, T.; Seeger, W. Investigation of the proinflammatory potential of biodegradable nanoparticle drug delivery systems in the lung. *Toxicol. Appl. Pharmacol.* **2006**, 215 (1), 100–108.
- (53) Jones, M.-C.; Jones, S. A.; Riffo-Vasquez, Y.; Spina, D.; Hoffman, E.; Morgan, A.; Patel, A.; Page, C.; Forbes, B.; Dailey, L. A. Quantitative assessment of nanoparticle surface hydrophobicity and its influence on pulmonary biocompatibility. *J. Controlled Release* **2014**, *183*, 94–104.
- (54) Valle, R. P.; Huang, C. L.; Loo, J. S. C.; Zuo, Y. Y. Increasing Hydrophobicity of Nanoparticles Intensifies Lung Surfactant Film Inhibition and Particle Retention. *ACS Sustainable Chem. Eng.* **2014**, 2 (7), 1574–1580.
- (55) Hu, G.; Jiao, B.; Shi, X.; Valle, R. P.; Fan, Q.; Zuo, Y. Y. Physicochemical properties of nanoparticles regulate translocation across pulmonary surfactant monolayer and formation of lipoprotein corona. *ACS Nano* **2013**, *7* (12), 10525–10533.
- (56) Hu, Q.; Bai, X.; Hu, G.; Zuo, Y. Y. Unveiling the Molecular Structure of Pulmonary Surfactant Corona on Nanoparticles. *ACS Nano* **2017**, *11* (7), 6832–6842.
- (57) Fan, Q.; Wang, Y. E.; Zhao, X.; Loo, J. S.; Zuo, Y. Y. Adverse biophysical effects of hydroxyapatite nanoparticles on natural pulmonary surfactant. ACS Nano 2011, 5 (8), 6410–6416.
- (58) Shi, X.; von dem Bussche, A.; Hurt, R. H.; Kane, A. B.; Gao, H. Cell entry of one-dimensional nanomaterials occurs by tip recognition and rotation. *Nat. Nanotechnol.* **2011**, *6* (11), 714–719.
- (59) Lin, X.; Zuo, Y.; Gu, N. Shape affects the interactions of nanoparticles with pulmonary surfactant. *Sci. China Mater.* **2015**, 58 (1), 28–37.
- (60) Possmayer, F.; Zuo, Y. Y.; Veldhuizen, R. A. W.; Petersen, N. O. Pulmonary Surfactant: A Mighty Thin Film. *Chem. Rev.* **2023**, DOI: 10.1021/acs.chemrev.3c00146.